Assessment of the variability of unidirectional prepregs at multiple scales

S. Gomarasca[1], S. M. A. Hosseini[1], R. Tao[1], B. Boos[2], C. Queck[2], D. Peeters[1], B. Atli-Veltin[1],

M. Gurka[2], C. Dransfeld[1]

[1]Delft University of Technology, Faculty of Aerospace Engineering, Department of Aerospace Structures and Materials,
Kluyverweg 1, 2629 HS Delft, The Netherlands
Email: S.Gomarasca@tudelft.nl, S.M.A.Hosseini@tudelft.nl, R.Tao@tudelft.nl, D.M.J.Peeters@tudelft.nl, B.Atli-veltin@tudelft.nl, C.A.Dransfeld@tudelft.nl
[2]Leibniz-Institut für Verbundwerkstoffe GmbH, Erwin-Schrödinger-Straße 58, 67663 Kaiserslautern, Germany
Email: Benedikt.Boos@ivw.uni-kl.de, Christoph.Queck@ivw.uni-kl.de, Martin.Gurka@ivw.uni-kl.de

Keywords: X-ray micro-computed tomography, microstructure analysis, multiscale analysis, structure tensor analysis, misalignment.

Abstract

Understanding the microstructural variability in unidirectional composite prepreg tapes is relevant to investigating mechanisms of tape microstructure formation, their impact on its processability and the mechanical performance of the final composite part. It has been shown that three-dimensional microstructural variability at the single-fibre level can be resolved by X-ray micro-computed tomography (XCT). However, to define a representative microstructural fingerprint of a given tape, investigations at the required small voxel size lead to limited volumes of observation, which might not be representative. This research aims to extend these findings via a multiscale approach, considering scales of observations, from microscopic (single fibre) up to mesoscopic (dimension of tape) length scale, to generate further insight into the microstructural organisation of thermoplastic prepreg tapes. By exploring the ability of XCT imaging for carbon fibre-reinforced thermoplastic composites at different voxel sizes, the work aims to identify the limitations of the use of different scales of observations to capture features of microstructures and their propagation from micro- to mesoscale level. While structure tensor analysis appeared to correctly capture misaligned regions in XCT images with small voxel size (1/10 of the fibre diameter), the method proved ineffective for larger voxel size images (1/2 of the fibre diameter).

Keywords: X-ray micro-computed tomography, microstructure analysis, multiscale analysis, structure tensor analysis, misalignment.

1 Introduction

Understanding the microstructural variability in unidirectional composite prepreg tapes, which are critical for the automation of large-scale composite production, is relevant for investigating mechanisms of microstructure formation and their impact on the processability and mechanical performance of the resulting composite part. Investigations based on X-ray micro-computed tomography (XCT) are becoming increasingly common in the field of composite characterisation to understand its three-dimensional (3D) variability. High-resolution XCT scans resolving individual fibres provide detailed microstructural information to identify relevant morphological characteristics in unidirectional composites. Approaches quantifying clustering effects in the fibre organisation [1], tortuosity of trajectories, bundling effects and 3D inter-connectivity in fibrous architecture [2] allow for local variability studies and highlight fine aspects of the level of organisation in the material. Evaluation of how processing or mechanical loading affects the microstructure can also be quantified, for example, in relation to debulking [3], bundle reorientation during compression loading [4], and kink band formation [5].

In manufacturing unidirectional composite prepregs, accurate microstructure characterisation is essential to identify local defects, such as regions of significant fibre misalignment. These features can adversely affect the mechanical performance of composites, particularly in terms of longitudinal stiffness and compressive strength [6, 7]. In high-fibre volume fraction tapes, individual highly tortuous or misaligned fibres can also influence the local organization of the surrounding microstructure, with their effects propagating over hundreds of micrometres [8]. While high-resolution XCT scans (with voxel size around 1/10th of the fibre diameter in our previous work on carbon fibres-reinforced tapes [2, 8, 9]) provide fine-scale details and allow clear visualization of single misaligned fibre effects, their limited field of view and long scan times make them impractical for analyzing large areas of tapes. These constraints, compounded by the high-resolution requirements of single-fibre tracking, limit the applicability of XCT for manufacturing quality screening and process optimization. Finding ways to identify single-fibre misalignment effects at a coarser resolution over larger areas would, therefore, help make XCT a more accessible technique for manufacturing quality screening. However, all these approaches have limitations due to the limited field of view, typically a few millimetres.

Structure tensor analysis is an image analysis technique that has been widely used in the study of fibre-reinforced composite materials due to its ability to capture fibre orientation distributions across a broad range of resolutions, with voxel sizes reported from approximately one to three fibre diameters in glass fibre composite laminates [10, 11]. Karamov et al. demonstrated the method's fidelity by comparing histograms of orientation angle components derived from single-fibre analysis and structure

tensor calculations. Their results showed a strong correlation, suggesting that structure tensor analysis is effective for evaluating local variability even at lower resolutions [10]. Jeppesen et al. used structure tensor analysis to compare fibre orientation variability in unidirectional carbon fibre prepreg laminates and pultruded profiles. The method effectively quantified differences in the standard deviation of fibre orientations, enabling meaningful comparative studies [12]. Furthermore, Ferguson et al. applied structure tensor analysis to evaluate kink band formation in pultruded carbon fibre composites at a resolution of 2 μm, showcasing its utility in identifying critical structural features [13]. Even though the applicability of structure tensor analysis is vast in the composites field, the specific case of free-standing unidirectional carbon fibre prepreg tapes has yet to be addressed in the literature.

Multiscale approaches might bridge the gap between high-resolution observations and macroscale variability in unidirectional composite tapes. Additionally, assessing information loss from varying voxel sizes is critical for ensuring that essential features of the microstructure are accurately represented. This research aims to investigate a multiscale approach in the case of unidirectional carbon fibre-reinforced thermoplastic tapes exposing misalignment areas to observe the propagation of defects in scans performed at different voxel sizes. By integrating observations across multiple scales, this work evaluates the effectiveness of state-of-the-art image analysis methods in quantifying variability at the fibre levels across different voxel sizes. To achieve this, low-voxel size scans were used to establish ground truth data for individual fibre tracking. These results were then compared with microstructural metrics resulting from the structure tensor method at coarser voxel sizes.

2 Materials and methods

2.1 Sample acquisition

To allow a multiscale approach for studying microstructural features in commercial carbon fibre-reinforced thermoplastic prepreg tapes, four samples measuring 25 mm by 25 mm were extracted from a 300 mm wide tape along the width direction. A schematic is shown in **Figure 1a**. Characterization was performed via XCT to generate datasets at different voxel sizes: 0.8 μm, 2 μm, and 3.5 μm. The XCT measurements were performed using a Zeiss Xradia Versa 520. Geometric magnification was optimized to achieve the desired total magnification in combination with either 0.4x or 4x optical magnification. A total of 2401 projections were acquired per scan, utilizing a 2024 x 2024 pixel CCD sensor operated without pixel binning. Volumetric data was reconstructed by Filtered Back Projection (FBP). The image acquisition settings used for the different magnifications are given in **Table 1**. For each sample, the scans for all magnifications were obtained in a single session to avoid misalignment between the scan volumes at different voxel sizes and to aid in identifying a common region of interest between the volumes at different voxel sizes. A cross-section of the region of interest considered for the following analysis is shown in **Figure 1b** for Sample 4 at all resolutions. For the measurement, the tapes were clamped at their bottom side and free-standing in air, visible in a darker colour at the top and bottom of the region of interest. Microporosity is present and distinguishable as darker regions through the tape cross-section, while fibres can be seen as lighter circles. The resulting sizes of the regions of interest for the four samples are reported in **Table 2**.
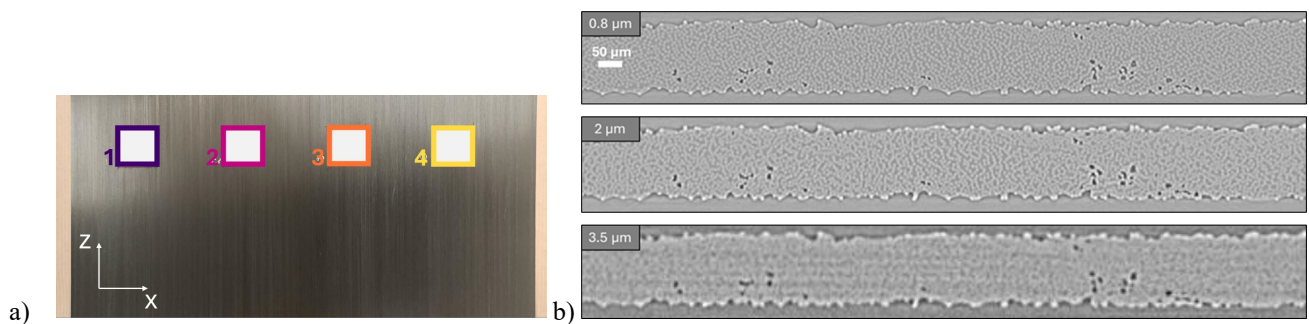

Figure 1: a) Schematic of the sample extraction from the unidirectional tape, with *z* fibre alignment direction and *x* direction along the tape width, b) For Sample 4, same transversal cross-section in the region of interest (*xy* plane) of overlap at the three voxel sizes considered.

Table 1: XCT volume acquisition parameters.

Voxel size (μm)	Voltage (kV)	Power (W)	Projections (-)	Exposure time (s)	Magnification (-)
0.8	80	7	2001	12.0	4x
2	80	7	2001	12.0	4x
3.5	80	7	2001	6.7	0.4x

Table 2: Size of the region of interest for the four samples. The direction *x* aligns to the tape width direction, *y* to the thickness, *z* to the fibre alignment direction. Dimensions were calculated based on the 0.8 μm dataset, and rounded to the nearest integer.

Direction	Sample 1	Sample 2	Sample 3	Sample 4
x (μm)	1526	1242	1546	1495
y (μm)	164	187	210	197
z (μm)	1084	1388	1400	1440

2.2 Microstructural analysis

The acquired volumes were manually registered in Fiji [14] to orient the tapes along their principal fibre alignment direction. The same region of interest was identified at all voxel sizes via manual volume selection.

The scanned samples showed microporosity. To aid in dedicated steps for the fibre architecture analysis, segmentation of fibres and pores was performed via the Fiji plugin Weka trainable Segmentation [14, 15]. Segmentation of the fibrous phase was conducted only on the 0.8 μm and 2 μm voxel size datasets since higher voxel size led to excessive homogenisation for fibre phase extraction. Pore information was used in this work to optimise the segmented fibre maps for artefact suppression. The segmented pores for the 0.8 μm and 2 μm voxel size scans were further processed by morphological filtering in Fiji via MorpholibJ [16] via 3D opening with a spherical element of radius size 2 and 1, respectively, for artefact removal, while further morphological operations were not done for the 3.5 μm scan.

2.2.1 Structure tensor analysis

Structure tensor analysis captures local orientations in the image with a variation in image intensity via applying gradient operations. The second-order structure tensor can be determined as:

$$\mathbf{S} = \sum \nabla \mathbf{V} \cdot \nabla \mathbf{V}^{\mathbf{T}} \tag{1}$$

The Gaussian derivative can be adopted to compute the intensity gradient V with a kernel size σ [12, 17], and the structure tensor is constructed by convolution with a Gaussian kernel Kρ:

$$S = K_\rho \cdot \nabla V_\sigma \cdot \nabla V_\sigma{}^T \tag{2}$$

In this formula, σ (smoothing scale) is the standard deviation of the Gaussian kernel to filter out the noise while calculating the gradient of image grayscale intensity, and ρ (integration scale) is the standard deviation of the Gaussian kernel Kρ for convolution of the result to select a specific range of the gradient. The formulation of the structure tensor used in this work follows the implementation by Jeppesen et al. [18]. Their code uses isotropic Gaussian kernels and a smoothing scale (σ) and integration scale (ρ) tailored to the voxel size and fibre diameter as follows:

$$\sigma = \sqrt{\frac{\left(R_f/v\right)^2}{2}} \tag{3}$$

$$\rho = 4 \cdot \sigma \tag{4}$$

where R_f is the fibre radius, and v is the voxel size. The values of σ and ρ (given in voxel) for the three voxel sizes considered are reported in **Table 3**. Since fibre structures have abrupt intensity variations across their transversal cross-section but almost zero intensity change in the longitudinal direction, their orientation can be determined as the direction of minimum grayscale intensity variation, attributed to the eigenvector corresponding to the smallest eigenvalue of the second-order structure tensor. In this work, the misalignment angle θ, ranging from 0° to 90°, is defined as the angle between the local material direction identified via the structure tensor and the principal fibre alignment direction *z*. In this work, we do not measure the azimuth angle on the *xy* plane as this is prone to high errors due to typically small angles θ, especially at high voxel size. A schematic is shown in **Figure 2**.

In the methodology used by Jeppesen et al. [17, 18], the structure tensor on the full 3D space is first calculated, followed by filtering with a mask based on the Otsu thresholding of the grayscale original volume, isolating the fibrous phase and excluding matrix regions presumed devoid of fibre directional information. However, the results were shown on images of the fully consolidated laminates in the absence of porosity or edges of the material, which, in the case of unidirectional tapes, becomes highly relevant due to their lower thickness and higher porosity content.
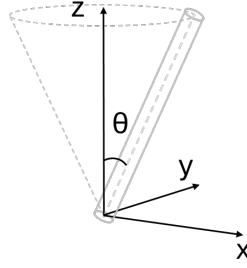
Figure 2: Schematic illustrating the definition of the misalignment angle θ of a straight fibre segment from the principal fibre alignment direction *z*.

Since in the case study considered in this work additional artefacts related to defects such as porosity were encountered, Otsu thresholding was substituted by the combination of the Otsu-thresholded probability map of segmented fibres derived from Weka segmentation and of the segmented pores. In addition, structural anisotropy was used as a filtering criterion for further artefact removal to correct for imperfections in the segmentation approach. The approach was employed in literature to aid in segmentation analysis of matrix and yarns of different orientations in carbon fibre-reinforced woven composites by considering anisotropy and orientation angle [19], and to segment tows, matrix pockets and pores in carbon fibre-reinforced unidirectional composite laminates [20]. The structural anisotropy was calculated at each voxel location as:

$$\beta = 1 - (\lambda_{min}/\lambda_{max}) \tag{5}$$

where λ_{min} and λ_{max} are, respectively, the maximum and minimum eigenvalues of the structure tensor at each voxel location. In case of high structural anisotropy, the value of β will tend to 1 ($\lambda_{min} \ll \lambda_{max}$), while in regions of low anisotropy β will tend to zero ($\lambda_{min} \sim \lambda_{max}$). In the case of unidirectional composites, the assumption justified by the literature is that regions with greater anisotropy should generally be more closely related to the fibrous microstructure [20]. In comparison, regions with lower anisotropy should indicate regions of porosity, matrix-rich areas and interfaces between the two. For the voxel size of 0.8 μm and 2 μm, an anisotropy threshold value of $\beta = 0.95$ was chosen. In the case of the 3.5 μm voxel size dataset, a value of $\beta = 0.88$ was selected as the threshold used for finer voxel sizes led to the exclusion of structure tensor values in large areas of tape, and a lower value was therefore deemed more suitable. The parameters for the three voxel size datasets and data refinement levels are summarized in **Table 3**.

Table 3: Selected values of the parameters used for the structure tensor analysis calculation and post-processing: smoothing scale (σ), integration scale (ρ), and anisotropy threshold value (β).

Processing	0.8 μm	2 μm	3.5 μm
unfiltered (U)	σ =3.09, ρ =12.36	σ =1.24, ρ =4.96	σ =0.71, ρ =2.84
segmentation masking (SM)	σ =3.09, ρ =12.36	σ =1.24, ρ =4.96	σ =0.71, ρ =2.84
segmentation masking + beta filtering (SMβ)	σ =3.09, ρ =12.36, β = 0.95	σ =1.24, ρ =4.96, β = 0.95	σ =0.71, ρ =2.84, β = 0.88

2.2.2 Single fibre analysis

The methodology for analysing low-voxel size scans at 0.8 μm was based on the method shown in our previous work, applied to the segmented fibre maps [2, 8, 9]. The segmented fibrous phase, optimised by further filtering from pore artefacts, allowed us to trace individual fibre paths with the Fiji plugin Trackmate [21]. The fibre trajectories were detected over 60 μm and further processed in Matlab to interpolate missing data linearly via the function '*fillmissing*' and smooth them via the function '*smooth*' with a 2nd-order polynomial and an interpolation length of 50 μm. Since the kernel radius used here for structure tensor analysis for all datasets has a diameter of $[2 \cdot 4 \cdot \rho \cdot v]$ = 79.36 μm, a comparable measure of the angular misalignment from the principal alignment direction for each detected fibre was determined locally at each detected traces fibre location with a moving window of 80 μm.

3 Results and discussion

3.1 Single fibre analysis

The method described in **Section 2.2.2** for single fibre trajectory extraction was only applied to the 0.8 μm voxel size dataset. For the 2 μm voxel size dataset, tracking was not successful, as segmentation led to large connected regions of fibres that could not be effectively separated into entities which could be traced via Trackmate. Consequently, fibre tracking was not attempted for the 3.5μm voxel size dataset.

The material variability across the different samples analysed is shown in **Figure 3**. The presence of highly misaligned regions can be observed in **Figure 3a** for Sample 4, where each 3D fibre trajectory is projected on the transversal cross-sectional plane and is colour-coded depending on its maximum local misalignment value. Highly misaligned fibres are shown in a darker colour and can be observed at the tape's top and bottom surfaces, as well as in discrete locations through the tape thickness. The histogram in **Figure 3b** displays all local misalignment values calculated at each point of the extracted fibre trajectories over an axial length of 80 μm, which highlights microstructural variability within each sample, with an initial peak for all samples at low local misalignment angles and a tail towards high misalignment angles up to angles of about 40°. While the majority of the local 3D fibre segments analysed have low misalignment values, which is expected in the case of an unidirectional composite tape, the presence in the fibre architecture of regions of higher misalignment is a relevant microstructural feature to highlight since they negatively impact the longitudinal strength of the material [6] and its stiffness [7], with higher likelihood of fracture initiation [22].
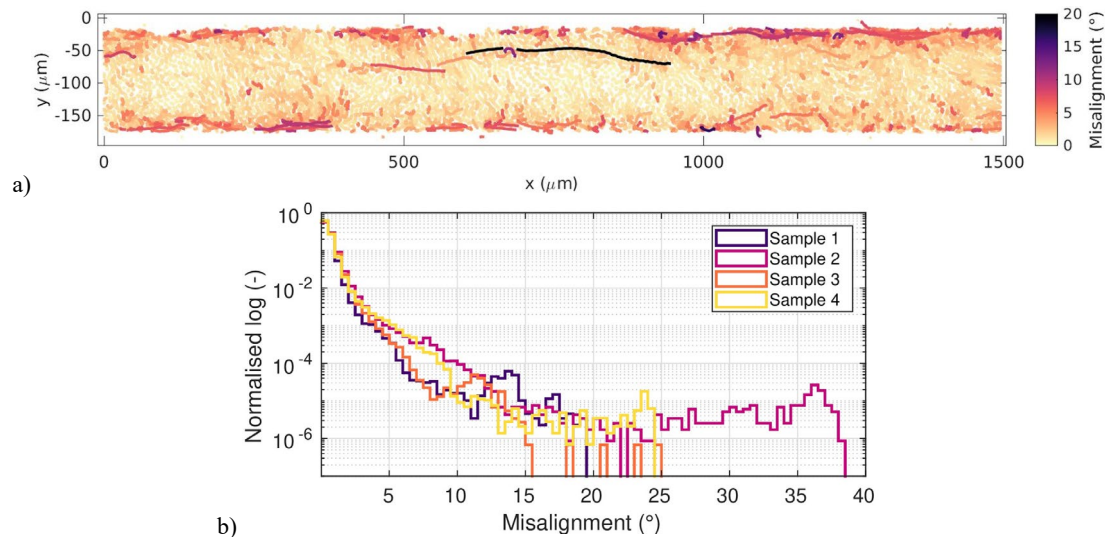

Figure 3: a) Consolidated view of the 3D misalignment distribution at a single fibre level for Sample 4 in the 0.8 μm voxel size dataset, where each fibre is projected on the transversal cross-section and colour-labelled with its maximum local misalignment value b) Histogram of the local misalignment range for Samples 1-2-3-4 at a 0.8 μm voxel size.

3.2 Structure tensor analysis

Three procedures of the structure tensor analysis are compared at first. As summarized in **Table 3**, the unfiltered misalignment (U), misalignment after segmentation masking (SM), and misalignment after segmentation masking with anisotropic filtering (SMβ) are three levels of refinement of the structure tensor output which affect the range of the obtained fibre orientations. Exemplarily, Sample 4 at 2 μm voxel size is shown in **Figure 4**.

To visualize 3D fibre orientations in a 2D representation, the maximum misalignment angle θ along the z-axis at each transversal cross-section location is shown for the three levels of data refinement in **Figure 4a-c**. In the unfiltered misalignment dataset (U), structure tensor calculations reveal artifact-laden fibre orientation information, particularly outside the tape region (e.g., in air) or in areas with complex features such as pores and matrix boundaries, where sharp angular variations occur and are translated by structure tensor calculation in high-angle values. Masking the structure tensor values using segmented volumes (SM) and applying anisotropic filtering (SMβ) effectively reduced these artefacts while preserving regions of high fibre misalignment observed in similar cross-sectional locations as identified in the single fibre analysis (**Figure 3a**).

While only consolidated cross-sectional data for Sample 4 are shown, the histogram comparison in **Figure 4d** shows quantitatively the impact of masking on the 3D structure tensor values on all samples, highlighting a common trend: anisotropic filtering significantly reduced the range of high-misalignment values detected, restricting the upper limit to approximately 15–27° across all datasets. While the range of angles obtained after SMβ filtering was relatively consistent for Samples 1, 3, and 4 with the results obtained via single fibre analysis, the structure tensor method did not accurately capture the full range of misalignment values for Sample 2, which single-fibre analysis revealed to extend up to ~40°. Further investigation is needed to refine the threshold values for anisotropic filtering and assess their influence on the observed microstructural features and the extent to which it might inadvertently mask significant misalignment features when the proximity of high misaligned fibres and matrix-pore interfaces occurs.

To evaluate more in detail the reliability of the methodology used to represent the cross-sectional distribution of maximum misalignment angles θ, Sample 4 after SMβ masking was here reported for the three datasets at 0.8 μm, 2 μm, and 3.5 μm voxel size (**Figure 5a1–a3**). The structure tensor successfully captured features such as edge-core effects in the cross-sectional

misalignment distribution at the finest voxel size (0.8 μm, ~10 voxels across the fibre diameter). However, the high-misalignment region in the tape bulk (600–800 μm width, **Figure 5a1**) displayed a lower range of values compared to single-fibre trajectory analysis (**Figure 3a**), indicating potential limitations in the accuracy of misalignment angles derived from the structure tensor. This discrepancy was also evident in the histograms (**Figure 4d** versus **Figure 3b**), where the structure tensor yielded lower maximum misalignment values than single-fibre analysis.
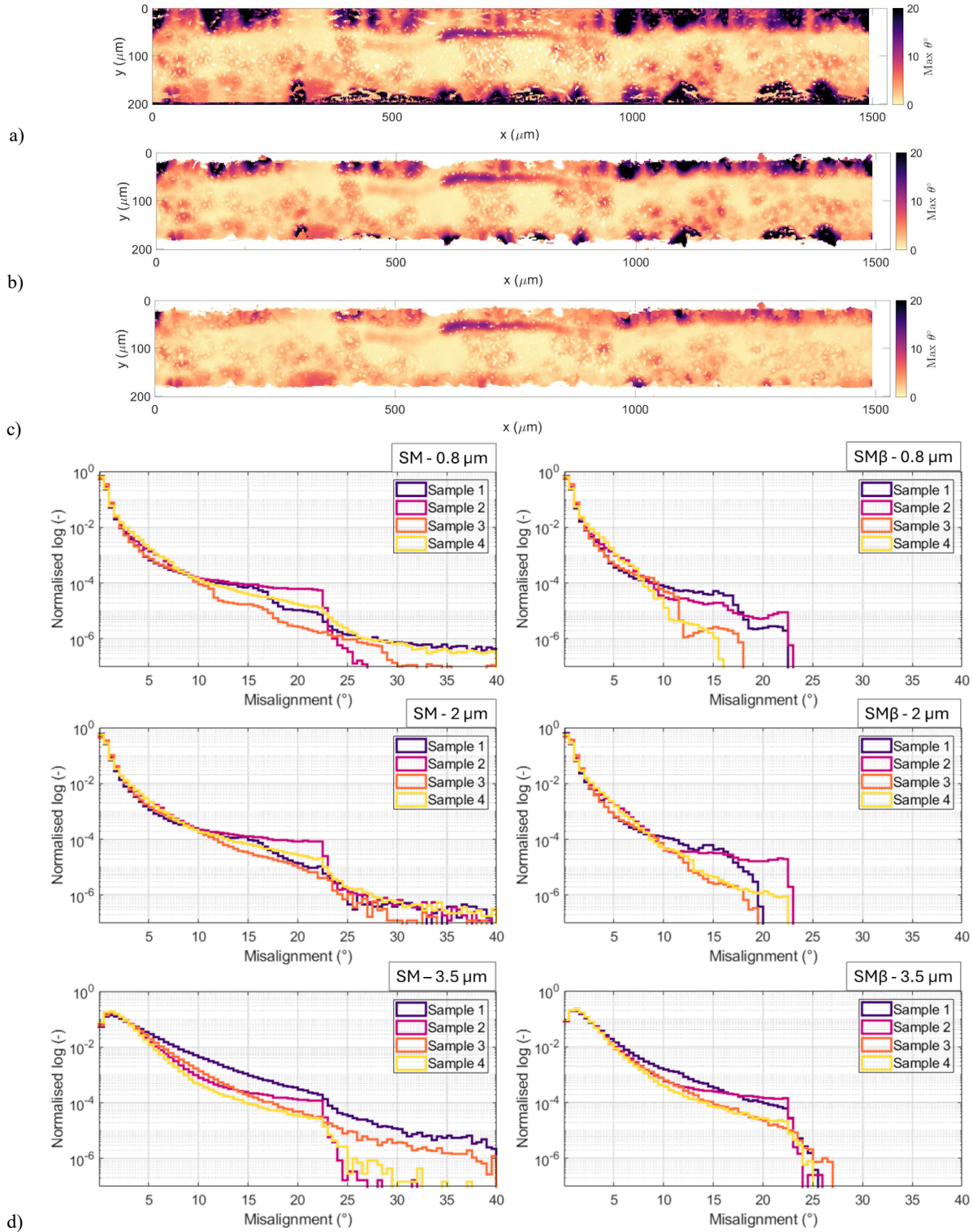

a)

b)

c)

d)

Figure 4:Consolidated view of the 3D structure tensor via its maximum value for each location on the *xy* plane for the 2 μm voxel size scan of Sample 4: a) before filtering b) after filtering with a mask based on fibres and pores segmentation c) after anisotropic filtering; d) histogram of the full range of misalignment angles derived from structure tensor for Samples 1-2-3-4, after segmentation masking (SM) and after anisotropic filtering (SMβ).

For larger voxel sizes, the visibility of fine features diminished, and noise increased. At 2 μm (~3 voxels across the fibre diameter, **Figure 5a2**), analysis uncertainty rose, with the structure tensor showing "bleeding" effects into surrounding areas [**12**], resulting in an inflated cross-sectional distribution of high-misalignment values. At 3.5 μm (~2 voxels across the fibre diameter, **Figure 5a3**), noise and discretization errors led to overestimated misalignment values, as reflected in histograms (**Figure 4d**). A noticeable shift in the distribution peak for low misalignment toward ~2° was observed and further quantified in **Figure 5b**, which reports the mean values of the full 3D misalignment distribution derived from both structure tensor and single fibre analysis. The standard deviation of the 3D misalignment values also shows a distinct increase in all 3.5 μm datasets compared to lower voxel sizes as shown in **Figure 5c**, which is consistent with the observations of Straumit et al. [**19**] in steel-epoxy unidirectional composites at a same voxel size-to-fibre diameter ratio. The effects observed are likely due to approaching the Nyquist limit affecting resolution and precise identification of low-misalignment regions. While the number of sampling voxels per fibre, as well as the noise and contrast levels in the image, are expected to influence the resolution of fibre features, it is possible that the appropriate scan coarseness for reliably resolving these features is determined not solely by fibre diameter but also by inter-fibre distance, and therefore depends on the characteristics of the heterogeneous morphology. This tape exhibits several regions of close fibre packing, as qualitatively observed in the cross-section of **Sample 4** in **Figure 1**. In contrast, other carbon-fibre-reinforced unidirectional prepregs with lower fibre volume fraction and greater inter-fibre spacing may allow for scans across a wider range of voxel sizes where fibres remain sufficiently resolved for tensor evaluation (and for single-fibre tracing, as described in **Section 3.1**).

While these considerations are based on 3D histogram distributions of misalignment values and their consolidated 2D representations, future work should delve deeper into the 3D spatial relationships of misalignment values and their propagation through the volume to assess with greater detail the differences in accuracy of the methods used (single fibre and structure tensor) in the local misalignment values identification at a 3D level. Additionally, there is not a clear agreement on an analytical definition of smoothing and integration scales, as different formulations were reported in the literature [**11, 17**], which optimisation could enable more effective feature extraction from datasets with higher voxel sizes, as suggested in the literature [**11 - 13**].
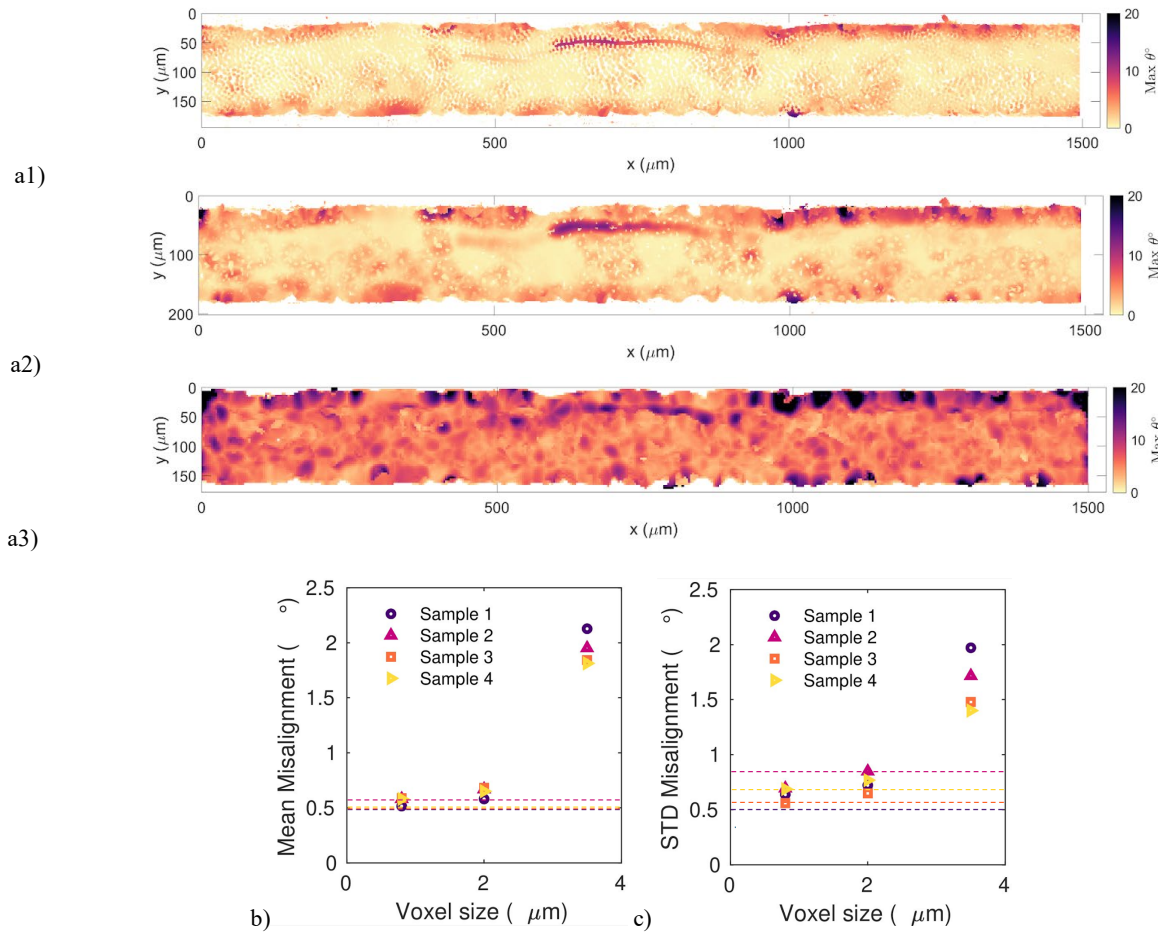

Figure 5: Consolidated view of the misalignment angle ϑ derived from the 3D structure tensor via its maximum value for each location on the *xy* plane for Sample 4 at different voxel sizes after SMβ filtering: a1) 0.8 μm a2) 2 μm a3) 3.5 μm; b-c) mean and standard deviation (STD) of the 3D misalignment values obtained via structure tensor analysis (symbols in the legend) and from single fibre analysis (horizontal lines following the same colour-coding).

4 Conclusion

This study demonstrated a novel methodology for assessing microstructural variability in unidirectional carbon fibre-reinforced tapes using multiscale XCT imaging. By systematically varying voxel sizes, we identified critical thresholds for fiber-level analysis. Single fibre reconstruction was feasible only at the smallest voxel size (0.8 μm, ~1/10th of the fibre diameter). At the same time, structure tensor analysis extended the capability to observe effects related to single fibre misalignment phenomena to voxel sizes up to 2 μm (~1/3rd of the fibre diameter). Even if the cross-sectional distribution of maximum misalignment values displayed for one of the samples showed close qualitative similarities to the distribution obtained at a single fibre level, differences in the value range in the high-misalignment regions were observed in structure tensor misalignment values, highlighting possible limitations of the method in accurate angle determination. Larger voxel sizes (3.5 μm, ~1/2 of the fibre diameter) were unsuitable for misalignment evaluation via structure tensor due to excessive local homogenization most likely due to approaching the Nyquist limit for fibre features, leading to significant information loss. Key challenges in the structure tensor analysis at all voxel sizes included artefacts caused by phase boundaries and air gaps interpreted as high misalignment, most likely due to the sharp directionality variations in those tape regions. The novelty of combining machine-learning-based segmentation strategies with filtering via structure tensor eigenvalue anisotropy reduced high-angle artefacts and proved essential for accurately highlighting areas populated by misaligned fibres. In this context, optimization of segmentation techniques and anisotropic filtering thresholds should be pursued to enhance the precision of feature extraction.

To summarise, while fine voxel size scans are still the standard for the analysis of fine microstructural features related to single fibre misalignment in unidirectional composite tapes, structure tensor analysis shows potential for bringing the analysis to a mesoscale level, potentially allowing to follow feature propagation over larger regions and reducing the requirements for XCT scanning. The findings offer recommendations for selecting appropriate voxel sizes depending on the level of detail required, as reported in **Table 4** as a practical guidance to researchers and practitioners. Within the Nyquist limit for feature detection, the limits of data processing for the voxel size reported in this study could possibly be relaxed to higher values in tapes with lower fibre volume fraction and greater inter-fibre spacing, which in these samples is observed to be qualitatively lower than the fibre diameter and might be a limiting factor in feature resolution. The adequate scan coarseness might, therefore, be highly dependent on the characteristics of the heterogeneous morphology. Future work should address the 3D spatial relationships between local fibre misalignment and larger microstructural phenomena with statistical rigour. Such insights could inform the development of predictive models linking single-fibre behaviours to bulk material properties, ultimately aiding in optimising tape manufacturing processes for improved mechanical performance.

Table 4: Summary of methods used for fibre misalignment analysis at different voxel sizes.

Method	0.8 μm	2 μm	3.5 μm
Single fibre trajectory analysis	Successful	Unsuccessful	Unsuccessful
Structure tensor analysis	Successful	Successful	Unsuccessful

References

[1] Schey, M. J., Beke, T., Appel, L., Zabler, S., Shah, S., Hu, J., Liu, F., Maiaru, M., and Stapleton, S., "Identification and Quantification of 3D Fiber Clusters in Fiber-Reinforced Composite Materials," JOM ,Vol. 73, 2021, pp. 2129–2142.

[2] Gomarasca, S., Peeters, D., Atli-Veltin, B., and Dransfeld, C.,"Characterising microstructural organisation in unidirectional composites," Composites Science and Technology, Vol. 215, No. July, 2021,pp. 109030.374.

[3] Schey, M., Beke, T., Owens, K., George, A., Pineda, E., and Stapleton, S., "Effects of debulking on the fiber microstructure and void distribution in carbon fiber reinforced plastics," Composites Part A, 2023, pp. 107364.378

[4] Emerson, M. J., Dahl, V. A., Conradsen, K., Mikkelsen, L. P., and Dahl, A. B., "Statistical validation of individual fibre segmentation from tomograms and microscopy," Composites Science and Technology, Vol. 160, No. January, 2018, pp. 208–215.

[5] Nelms, K., Paul, P., Wowogno, A., Chen, Y., Lukic, B., Rack, A., Chandarana, N., and Withers, P., "Effect of fibre orientation on compression micromechanics in CFRP investigated by computed tomography," Twenty-Third International Conference On Composite Materials (ICCM23). Queen's University Belfast, University Road, Belfast, Northern Ireland, BT7 1NN, 12 p., 2023.

[6] Xie, C., Meng, Y., Chen, J., Zhao, Z., Wang, J., Jiang, J., and Li, Y.,"Interaction of multiple micro-defects on the strength and failure mechanism of UD composites by computational micromechanics," Composite Structures, Vol. 349–350, 2024, pp. 118492.

[7] Liu, N. and Chen, P., "A three-dimensional failure criterion model considering the effects of fiber misalignment on longitudinal tensile failure,"Composites Science and Technology, Vol. 247, 2024, pp. 110424.

[8] Gomarasca, S., Peeters, D., Slange, T., Ratouit, G., Atli-Veltin, B., and Dransfeld, C., "Characterising pore networks and their interrelation with the fibre architecture in unidirectional composites," Composites Part A: Applied Science and Manufacturing, 2025 (under review)

[9] Gomarasca, S., Peeters, D. M. J., Atli-Veltin, B., Dransfeld, C. A., and Luinge, H., "The role of matrix boundary in the microstructure of unidirectional composites," Proceedings of the 20th European Conference on Composite Materials - Composites Meet Sustainability, Vol. 3, 2022,pp. 636–643.

[10] Karamov, R., Martulli, L. M., Kerschbaum, M., Sergeichev, I., Swolfs, Y., and Lomov, S. V., "Micro-CT based structure tensor analysis of fibre orientation in random fibre composites versus high-fidelity fibre identification methods," Composite Structures, Vol. 235, No. November 2019, 2020, pp. 111818.

[11] Auenhammer, R. M., Prajapati, A., Kalasho, K., Mikkelsen, L. P., Withers, P. J., Asp, L. E., and Gutkin, R., "Fibre orientation distribution function mapping for short fibre polymer composite components from low resolution/large volume X-ray computed tomography," Composites Part B: Engineering, Vol. 275, 2024, pp. 111313.

[12] Jeppesen, N., Mikkelsen, L. P., Dahl, A. B., Christensen, A. N., and Dahl, V. A., "Quantifying effects of manufacturing methods on fiber orientation in unidirectional composites using structure tensor analysis," Composites Part A, Vol. 149, No. July, 2021, pp. 106541.

[13] Ferguson, O., Skovsgaard, S., Jensen, H., and Mikkelsen, L., "Compressive strength prediction of carbon fiber-reinforced pultruded profiles including realistic volumetric fiber orientations," European Journal of Mechanics - A/Solids, Vol. 104, Supplement, 2024, pp. 105011.

[14] Schindelin, J., Arganda-Carreras, I., Frise, E., Kaynig, V., Longair, M., Pietzsch, T., Preibisch, S., Rueden, C., Saalfeld, S., Schmid, B., Tinevez, J. Y., White, D. J., Hartenstein, V., Eliceiri, K., Tomancak, P., and Cardona, A., "Fiji: An open-source platform for biological-image analysis," Nature Methods, Vol. 9, No. 7, 2012, pp. 676–682.

[15] Arganda-Carreras, I., Kaynig, V., Rueden, C., Eliceiri, K. W., Schindelin, J., Cardona, A., and Seung, H. S., "Trainable Weka Segmentation: A machine learning tool for microscopy pixel classification," Bioinformatics, Vol. 33, No. 15, 2017, pp. 2424–2426.

[16] Legland, D., Arganda-Carreras, I., Andrey, P., and MorphoLibJ, "MorphoLibJ: integrated library and plugins for mathematical morphology with ImageJ," Bioinformatics, Vol. 22, 2016, pp. 3532–3534.

[17] Jeppesen, N., Dahl, V. A., Christensen, A. N., Dahl, A. B., and Mikkelsen, L. P., "Characterization of the fiber orientations in non-crimp glass fiber reinforced composites using structure tensor," IOP Conf. Series: Materials Science and Engineering, Vol. 492, 2020, pp. 012037.

[18] Legland, D., Arganda-Carreras, I., Andrey, P., "MorphoLibJ: integrated library and plugins for mathematical morphology with ImageJ," Bioinformatics, 32(22), 2016; 3532-3534.

[19] Straumit, I., Lomov, S. V., and Wevers, M., "Quantification of the internal structure and automatic generation of voxel models of textile composites from X-ray computed tomography data," Composites Part A: Applied Science and Manufacturing, Vol. 69, 2015, pp. 150–158.

[20] Nguyen, N. Q., Mehdikhani, M., Straumit, I., Gorbatikh, L., Lessard, L., and Lomov, S. V., "Micro-CT measurement of fibre misalignment: Application to carbon/epoxy laminates manufactured in autoclave and by vacuum assisted resin transfer moulding," Composites Part A: Applied Science and Manufacturing, Vol. 104, 2018, pp. 14–23.

[21] Tinevez, J. Y., Perry, N., Schindelin, J., Hoopes, G. M., Reynolds, G. D., Laplantine, E., Bednarek, S. Y., Shorte, S. L., and Eliceiri, K. W., "TrackMate: An open and extensible platform for single-particle tracking," Methods, Vol. 115, 2017, pp. 80–90.

[22] Fast, T., Scott, A. E., Bale, H. A., and Cox, B. N., "Topological and Euclidean metrics reveal spatially nonuniform structure in the entanglement of stochastic fiber bundles," Journal of Materials Science, Vol. 50, No. 6, 2015, pp. 2370–2398.